ELECTRONIC SUPPORTING INFORMATION

Membrane Partition of *bis*-(3-hydroxy-4-pyridinonato) zinc(II) Complexes Revealed by Molecular Dynamics Simulations

João T. S. Coimbra,[a] Natércia F. Brás,[a] Pedro A. Fernandes,[a] Maria Rangel,[b,] Maria J. Ramos[a,]**

[a] UCIBIO, REQUIMTE, Departamento de Química e Bioquímica, Faculdade de Ciências, Universidade do Porto, Rua do Campo Alegre, s/n, 4169-007 Porto, Portugal

[b] LAQV, REQUIMTE, Instituto de Ciências Biomédicas de Abel Salazar, Universidade do Porto, Rua de Jorge Viterbo Ferreira nº 228, 4050-313 Porto, Portugal

Parameterization of Zn(II) complexes. In Figure ESI-1 we present the structure used in the parameterization of the Zn(II) complexes studied here. The resulting structure was used as a skeleton for the generation of the other complexes. A gas-phase geometry optimization was performed in the represented structure, and linear transit scans were also performed in the presence of the two additional X-ray water molecules (that were not coordinated to the metal). These two water molecules were excluded from the RESP charge generation protocol, which was also performed in gas-phase. The inclusion of the two additional water molecules was a necessity, to

maintain the overall geometry of the metal center; otherwise, the coordinated water ligand would strongly interact with the other oxygen donor atoms (upon optimization of the structure). The protocol was the same for the other Zn(II) complexes. The tetra-coordinated Zn(II) complex 2 was also parameterized following the same approach, without the inclusion of the water molecules.

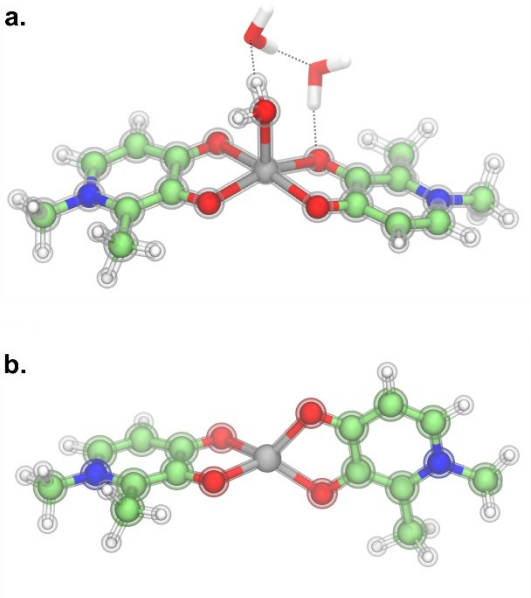

Figure ESI-1. Representation of the X-ray DFT-optimized structures. **a.** penta-coordinated [Zn(II)(dmpp)$_2$Wat] complex; and **b.** the tetra-coordinated [Zn(II)(dmpp)$_2$] complex. Two additional (non-metal coordinated) water molecules were included in the gas-phase optimization of the former complex and for the linear transit scans of bonds and angles involving zinc. RESP charge derivation protocol was employed in the transparency-highlighted structure (excluding the two X-ray water molecules). Hydrogen bond interactions with X-ray water molecules are also highlighted.

Partition errors. The errors for the results shown in Table 1 (binding free energies, partition, and permeability estimates), where derived from the PMFs' errors originated from the bootstrapping analysis. For the binding free energy error, the binding energies were determined for each bootstrap-generated PMF (200 total profiles per compound); these were sorted in ascending order, and finally grouped in 10 blocks. Then we calculated the standard deviation of the mean (σ_M), using the following formula: $\left[1/(M-1)\sum_{j=1}^{M}(\mu_j-\bar{\mu})^2\right]^{1/2}$, for M estimates of the mean, μ, with overall mean $\bar{\mu}$.[1] The partition coefficient and permeability estimate errors were determined through error propagation analysis.

Membrane models and their stability. The stability of the membrane models was assessed by a few structural and dynamical membrane properties: area per lipid (A_L), head-to-head bilayer thickness (D_{HH}), order parameters of the acyl chains (S_{CD}), electron density profiles, lipid lateral diffusion coefficients (D_l), and isothermal area compressibility modulus (K_A). In Table ESI-1, we present the results for the A_L, D_{HH}, and D_l properties over the last 20 ns of the equilibration MD simulations, considering the two membrane models employed in this study: i) the 32:32 system; and ii) the 150:150 system. We also show the simulated values for the K_A property, but in this case, the last 80 ns of the 100 ns MD simulations were considered in the analysis. As described by others,[2] it is very difficult to obtain accurate results for the isothermal area compressibility property, K_A. Normally, relatively large simulations (0.5 μs or more) are needed for a good agreement with the experiment, even in smaller systems. Available experimental results are also presented, together with the temperature conditions of the experiments and simulations.[3–8]

Table ESI-1. Structural (area per lipid – A_L, head-to-head bilayer thickness - D_{HH}, K_A - isothermal area compressibility modulus) and dynamical (lipid diffusion coefficients - D_l) properties are hereby presented for each bilayer system. i) is indicative of the 32:32 system, and ii) of the 150:150 system. The analysis of these parameters comprises the last 20 ns of the MD simulation of the equilibration stage, except for the K_A property, where the last 80 ns were considered. Experimental results are also depicted together with the temperature conditions of the experiments.

lipid	T / K	A_L / nm^2			D_{HH} / nm			D_l / 10^{-8}·cm^2·s^{-1}			K_A / mN·m^{-1}		
		sim. i)	sim. ii)	exptl.	sim. i)	sim. ii)	exptl.	sim. i)	sim. ii)	exptl.	sim. i)	sim. ii)	exptl.
DMPC	303	-	-	0.599	-	-	3.44, 3.53	-	-	5.95, 9.00	-	-	234 ± 23, 257
	310	0.604	0.612	-	3.56	3.50	-	6.80	8.90	-	267 ± 19	252 ± 34	-
	323	-	-	0.633	-	-	-	-	-	22.3	-	-	-

Order parameters of the lipid tails were also assessed. These are plotted in Figure ESI-2. We see that the order parameters are below 0.30, which is characteristic of a disordered lipid phase, in accordance with the expected behavior at 310 K for this lipid system. Experimental order parameters are also presented.[9]

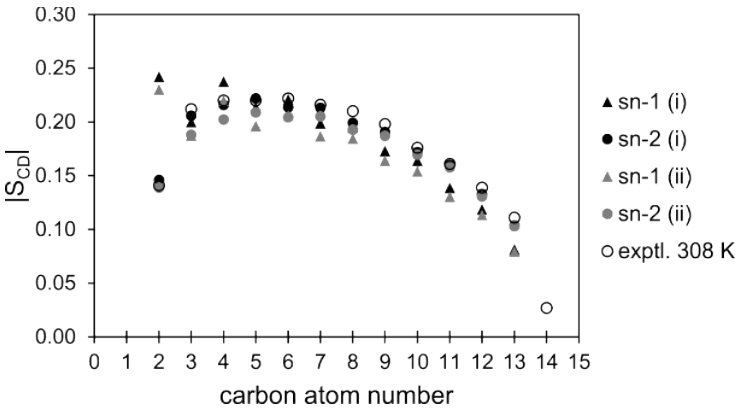

Figure ESI-2. Order parameters ($|S_{CD}|$) considering the last 20 ns of the equilibration MD simulation. Experimental data reflects the results of the sn-2 chain at 308 K.

Electron density profiles were used to assess the D_{HH}, through the phosphate group peak-to-peak distance between both layers. We only show in Figure ESI-3 the profile for the 150:150 bilayer system, as no marked differences were detected between the two employed bilayers. The density of other important lipid moieties is also depicted.

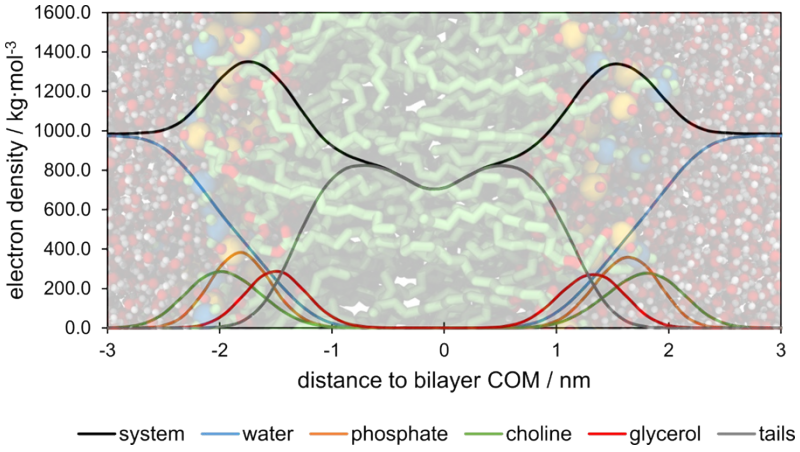

Figure ESI-3. Electron density profile of the last 20 ns of the equilibration MD simulation for the 150:150 system. The density profiles presented here include the contribution from hydrogen atoms, when present in the phospholipid's chemical groups. The terminology used for the phospholipids' groups is derived from the parent molecules or functional groups that establish

each phospholipid group. A membrane representation is added in the background of the density profile.

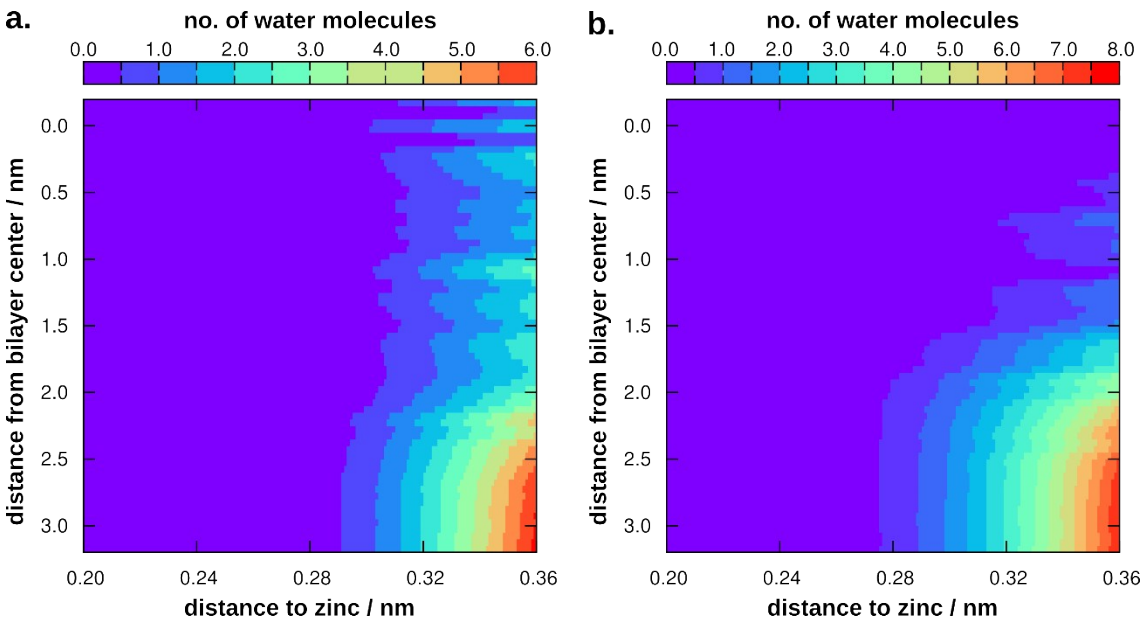

Figure ESI-4. The number of water molecules as a function of the distance to the zinc atom (xx axis) and as a function of the distance from the bilayer center (yy axis). **a.** Number of water molecules considering the [Zn(dmpp)$_2$Wat] complex. **b.** number of water molecules considering the [Zn(dmpp)$_2$] complex.

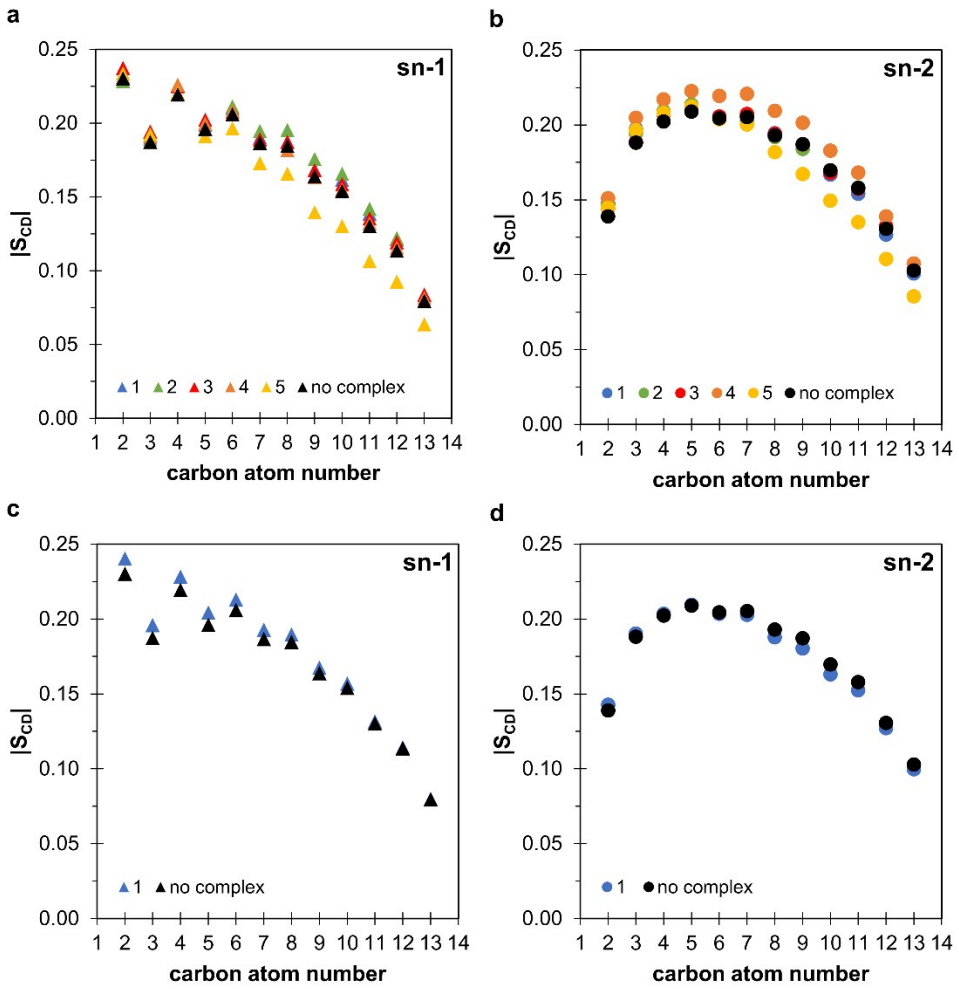

Figure ESI-5. Order parameters ($|S_{CD}|$) considering the last 20 ns of the cMD simulations. **a.** and **b.** sn-1 chain and sn-2 order parameters for the cMD simulations of the 32:32 lipid systems, in the presence and absence of zinc(II) complexes (one complex per system); **c.** and **d.** sn-1 and sn-2 order parameters for the cMD simulations of the 150:150 lipid systems, in the presence and absence of eight $[Zn(mpp)_2Wat]$ complexes.

Table ESI-2. The area per lipid (A_L) of the 32:32 lipid systems, in the presence of zinc(II) complexes. The A_L in the absence of zinc(II) complexes is also shown for comparison.

complex	A_L / nm^2
no complex	0.604 ± 0.016
$[Zn(mpp)_2Wat]$	0.614 ± 0.018
$[Zn(dmpp)_2Wat]$	0.611 ± 0.017
$[Zn(depp)_2Wat]$	0.624 ± 0.014
$[Zn(heepp)_2Wat]$	0.602 ± 0.016
$[Zn(hexylmpp)_2Wat]$	0.631 ± 0.017

REFERENCES

1 C. Neale, W. F. D. Bennett, D. P. Tieleman and R. Pomès, Statistical convergence of equilibrium properties in simulations of molecular solutes embedded in lipid bilayers, *J. Chem. Theory Comput.*, 2011, **7**, 4175–4188.

2 J. P. M. Jämbeck and A. P. Lyubartsev, Derivation and Systematic Validation of a Refined All-Atom Force Field for Phosphatidylcholine Lipids, *J. Phys. Chem. B*, 2012, **116**, 3164–3179.

3 N. Kučerka, M.-P. Nieh and J. Katsaras, Fluid phase lipid areas and bilayer thicknesses of commonly used phosphatidylcholines as a function of temperature, *Biochim. Biophys. Acta - Biomembr.*, 2011, **1808**, 2761–2771.

4 N. Kučerka, Y. Liu, N. Chu, H. I. Petrache, S. Tristram-Nagle and J. F. Nagle, Structure of Fully Hydrated Fluid Phase DMPC and DLPC Lipid Bilayers Using X-Ray Scattering from Oriented Multilamellar Arrays and from Unilamellar Vesicles, *Biophys. J.*, 2018, **88**, 2626–2637.

5 H. I. Petrache, S. Tristram-Nagle and J. F. Nagle, Fluid phase structure of EPC and DMPC bilayers, *Chem. Phys. Lipids*, 1998, **95**, 83–94.

6 P. F. F. Almeida, W. L. C. Vaz and T. E. Thompson, Lateral diffusion in the liquid phases of dimyristoylphosphatidylcholine/cholesterol lipid bilayers: a free volume analysis, *Biochemistry*, 1992, **31**, 6739–6747.

7 G. Orädd, G. Lindblom and P. W. Westerman, Lateral Diffusion of Cholesterol and Dimyristoylphosphatidylcholine in a Lipid Bilayer Measured by Pulsed Field Gradient NMR Spectroscopy, *Biophys. J.*, 2002, **83**, 2702–2704.

8 A. Filippov, G. Orädd and G. Lindblom, Influence of Cholesterol and Water Content on Phospholipid Lateral Diffusion in Bilayers, *Langmuir*, 2003, **19**, 6397–6400.

9 J. P. Douliez, A. Léonard and E. J. Dufourc, Restatement of order parameters in biomembranes: calculation of C-C bond order parameters from C-D quadrupolar splittings, *Biophys. J.*, 1995, **68**, 1727–1739.